ADVANCED HEALTHCARE MATERIALS
www.advhealthmat.de

Prostate-Specific Membrane Antigen Targeted StarPEG Nanocarrier for Imaging and Therapy of Prostate Cancer

*Niranjan Meher, Gary W. Ashley, Kondapa Naidu Bobba, Anju Wadhwa, Anil P. Bidkar, Chandrashekhar Dasari, Changhua Mu, Ramya Ambur Sankaranarayanan, Juan A. Camara Serrano, Athira Raveendran, David P. Bulkley, Rahul Aggarwal, Nancy Y. Greenland, Adam Oskowitz, David M. Wilson, Youngho Seo, Daniel V. Santi, Henry F. VanBrocklin, and Robert R. Flavell**

The tumor uptake of large non-targeted nanocarriers primarily occurs through passive extravasation, known as the enhanced permeability and retention (EPR) effect. Prior studies demonstrated improved tumor uptake and retention of 4-arm 40 kDa star polyethylene glycol (StarPEG) polymers for cancer imaging by adding prostate-specific membrane antigen (PSMA) targeting small molecule ligands. To test PSMA-targeted delivery and therapeutic efficacy, StarPEG nanodrugs with/without three copies of PSMA-targeting ligands, ACUPA, are designed and synthesized. For single-photon emission computed tomography (SPECT) imaging and therapy, each nanocarrier is labeled with 177Lu using DOTA radiometal chelator. The radiolabeled nanodrugs, [177Lu]PEG-(DOTA)1 and [177Lu]PEG-(DOTA)1(ACUPA)3, are evaluated in vitro and in vivo using PSMA+ PC3-Pip and/or PSMA– PC3-Flu cell lines, subcutaneous xenografts and disseminated metastatic models. The nanocarriers are efficiently radiolabeled with 177Lu with molar activities 10.8–15.8 MBq/nmol. Besides excellent in vitro PSMA binding affinity (kD = 51.7 nM), the targeted nanocarrier, [177Lu]PEG-(DOTA)1(ACUPA)3, demonstrated excellent in vivo SPECT imaging contrast with 21.3% ID/g PC3-Pip tumors uptake at 192 h. Single doses of 18.5 MBq [177Lu]PEG-(DOTA)1(ACUPA)3 showed complete resolution of the PC3-Pip xenografts observed up to 138 days. Along with PSMA-targeted excellent imaging contrast, these results demonstrated high treatment efficacy of [177Lu]PEG-(DOTA)1(ACUPA)3 for prostate cancer, with potential for clinical translation.

1. Introduction

Prostate cancer is the most frequently diagnosed noncutaneous malignancy in men and is a worldwide public health concern. Prostate-specific membrane antigen (PSMA) or glutamate carboxypeptidase II (GCPII), a class II transmembrane glycoprotein, is an overexpressed enzyme on prostate cancer (PCa) cell membranes and serves as a well-validated clinical biomarker for PCa theranostics.[1] The isolation and analysis of the PSMA crystal structure in 2005 assisted the design of efficient low-molecular-weight PSMA inhibitors highly specific toward its enzymatic pocket.[2] The urea-based small molecule ligands DUPA and ((S)−2-(3- ((S)−5-amino-1-carboxypentyl) ureido) pentanedioic acid (ACUPA) with three carboxylic acid groups are potent PSMA inhibitors with high binding affinity and have been employed in developing several theranostic agents. In particular, the US Food and Drug Administration (FDA) approved [^{68}Ga]PSMA-11, [^{18}F]rhPSMA-7.3 and [^{18}F]DCFPyL, ureido-glutamate-based PSMA inhibitors, have been efficiently employed for PCa positron emission tomography (PET) imaging in the

N. Meher, K. N. Bobba, A. Wadhwa, A. P. Bidkar, C. Mu, R. A. Sankaranarayanan, A. Raveendran, D. M. Wilson, Y. Seo, H. F. VanBrocklin, R. R. Flavell
Department of Radiology and Biomedical Imaging
University of California
San Francisco, CA 94143, USA
E-mail: robert.flavell@ucsf.edu

The ORCID identification number(s) for the author(s) of this article can be found under https://doi.org/10.1002/adhm.202304618

DOI: 10.1002/adhm.202304618

N. Meher
National Institute of Pharmaceutical Education and Research
Raebareli
Lucknow, UP 226002, India

G. W. Ashley, D. V. Santi
ProLynx Inc.
San Francisco, CA 94158, USA

C. Dasari, A. Oskowitz
Helen Diller Family Comprehensive Cancer Center
University of California San Francisco
San Francisco, CA 94143-0981, USA

J. A. C. Serrano, R. Aggarwal, D. M. Wilson, Y. Seo, H. F. VanBrocklin, R. R. Flavell
Division of Vascular and Endovascular Surgery
University of California
San Francisco, CA 94143-0957, USA

clinic.[1] Another landmark success includes the approval of ACUPA conjugated small molecule agent, [^{177}Lu]PSMA-617, for the treatment of metastatic castration-resistant prostate cancer (mCRPC) by the FDA in 2022.[3] Numerous additional PSMA-targeting agents incorporating ACUPA and analogous ligands are in active clinical trials.[1,4] While the small molecule agents are highly effective, their fast pharmacokinetics limit the radiation exposure needed for therapy. Thus, for optimum therapeutic response, ACUPA-based radiotherapies can require multiple high-dose treatments, as seen for [^{177}Lu]PSMA-617.[1,5] These limitations motivated the development of nanocarrier systems with prolonged tumor retention as alternatives for cancer therapy to complement small-molecule approaches.[6]

The enhanced permeability and retention (EPR) effect is a well-established and debated phenomena associated with the delivery of large-size nanocarriers to tumors, in which passive tumor accumulation of the nanomedicines may be achieved as a result of permeable tumor vasculature and limited lymphatic drainage.[7,8] However, tumor vascularity of different cancer phenotypes is variable and several preclinical prostate cancer xenografts have shown poor vascularity.[8–10] Our previous studies describing 4-armed StarPEG radiopharmaceutical (40 kDa) of around 12 nm have demonstrated high retention in human colorectal adenocarcinoma (HT-29) and human breast adenocarcinoma (MX-1) tumor models but showed poor accumulation and heterogeneous intratumor distribution in prostate cancer models such as PC3.[11,12] In addition, similar studies using different nanocarrier systems demonstrated low and predominantly peripheral accumulation of large-size nanocarriers in multiple prostate cancer models including 22rv1, DU-145, and PC3.[13,14]

Therefore, it was hypothesized that the accumulation and tumor penetration of 40 kDa StarPEG nanocarriers in prostate cancer xenografts might be enhanced by conjugating PSMA-targeting ACUPA ligands, to improve therapeutic efficacy.[12] In PET imaging studies, StarPEG nanocarriers conjugated with ACUPA ligands demonstrated homogenous deep tissue penetration in PSMA+ PC3-Pip xenografts, whereas heterogenous peripheral accumulation was observed in PSMA− PC3-Flu tumors.[12] Therefore, it was believed that cognate therapeutic agents for radiopharmaceutical therapy represent a promising therapy for prostate cancer. In this study, the radiometal-chelate pair 89Zr-DFB (deferoxamine B) was replaced with ^{177}Lu-DOTA, used to label two theranostic StarPEG nanocarriers, PSMA-targeted [^{177}Lu]PEG-$(DOTA)_1(ACUPA)_3$ and non-targeted [^{177}Lu]PEG-$(DOTA)_1$. These two radiopharmaceuticals were evaluated for their PSMA-targeted theranostic efficacy against prostate cancer (**Figure 1**).

D. P. Bulkley
Department of Pathology
University of California
San Francisco, CA 94143, USA

N. Y. Greenland
Department of Pharmaceutical Chemistry
University of California
San Francisco, CA 94158-2517, USA

R. R. Flavell
Department of Biochemistry and Biophysics
University of California
San Francisco, CA 94158, USA

2. Results

2.1. Design and Synthesis of Theranostic StarPEG Conjugates

2.1.1. Design of StarPEG Conjugates

Due to poor vascularity of tumor xenografts, large nanocarriers undergo EPR-mediated heterogeneous and low peripheral passive accumulation in most prostate cancer tumor models.[6] Recently, several 40 kDa, 15 nm, diagnostic StarPEG nanocarriers were evaluated that demonstrated selectively improved tumor accumulation and penetration in PSMA+ PC3-Pip tumors by conjugating PSMA-targeting ACUPA ligands.[12] Herein, the therapeutic version of the StarPEG nanocarriers has been developed by replacing the diagnostic radiometal-chelator pair of ^{89}Zr-DFB with ^{177}Lu-DOTA. To elaborate the new radiopharmaceuticals, two StarPEG conjugates were designed with or without three copies of PSMA targeting ACUPA ligands, PEG-$(DOTA)_1$ and PEG-$(DOTA)_1(ACUPA)_3$ (Figure 1), in which both the nanocarriers were conjugated with one copy of DOTA to chelate the beta-emitting theranostic radiometal ^{177}Lu. The primary goal of this design strategy was to maximize the treatment efficacy in both PSMA+ subcutaneous and metastatic tumor models.

2.1.2. Synthesis and Characterization of StarPEG Conjugates

For the synthesis of the designed StarPEG nanocarriers, the previously synthesized and reported PEG-$(5HCyO)_3(NH2)_1$ was employed as starting material.[6,12] As summarized in **Scheme 1**, both the nontargeted nanocarrier [PEG-$(DOTA)_1$] and the targeted nanocarrier [PEG-$(DOTA)_1(ACUPA)_3$] were prepared following similar synthetic routes. PEG-$(5HCyO)_3(NH2)_1$ with three cyclooctyne counterparts were subjected to second-generation azide click reactions with either Azido-ACUPA or Azido-PEG7 to yield PEG-$(ACUPA)_3(NH_2)$ or PEG-$(PEG_7)_3(NH_2)$, respectively.[20] The intermediates were purified using 12–14 kDa cutoff dialysis membrane and were further reacted with isothiocyanatobenzyl-DOTA (ITCBz-DOTA) to produce the polymer conjugates of interest, i.e., either PEG-$(DOTA)_1$ or PEG-$(DOTA)_1(ACUPA)_3$. Post DOTA conjugation, the PEG conjugates were purified using 12–14 kDa cutoff dialysis membrane and dried under reduced pressure to give 93% and 91% yield for PEG-$(DOTA)_1$ and PEG-$(DOTA)_1(ACUPA)_3$, respectively. The conjugation of ACUPA and DOTA ligands to the polymer nanocarriers was confirmed by comparing their proton NMR (Figures S1 and S2, Supporting Information). Prominent peaks at around 4.45 and 4.26 ppm were observed in both the intermediates and final polymer conjugates after click conjugation of azido-PEG7 or Azido-ACUPA, respectively, that correspond to the CH_2 protons close to triazole. No peaks corresponding to CH_2 protons in the 4–4.5 ppm range were observed in the starting material PEG-$(5HCyO)_3(NH2)_1$. Furthermore, a noticeable aromatic peak at 7.21 ppm was observed after the

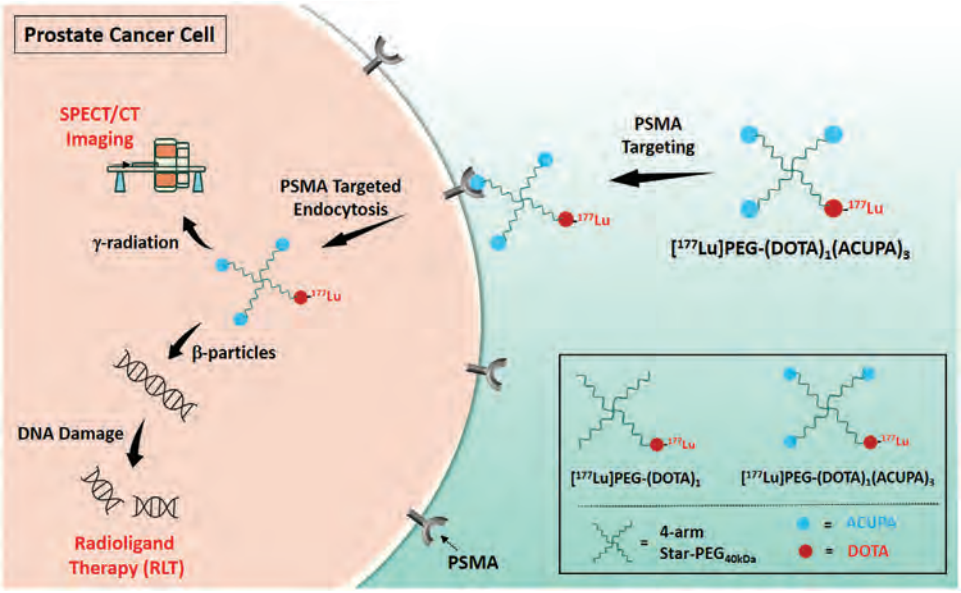

Figure 1. Graphical representation of prostate-specific membrane antigen (PSMA) targeted μSPECT (micro single-photon emission computed tomography)/CT imaging and therapy of prostate cancer using ^{177}Lu-labeled StarPEG nanocarrier.

conjugation of ITCBz-DOTA, which corresponds to the phenyl protons and confirms the conjugation of DOTA to the StarPEG nanocarriers. Transmission electron microscope images of the StarPEG conjugates were recorded that demonstrated the formation of nanoparticles in the range of 10–20 nm size (Figure S3, Supporting Information).

2.1.3. Radiolabeling of StarPEG Conjugates

The radiolabeling of ^{177}Lu to the DOTA conjugated StarPEG nanocarriers was performed in NH_4OAc buffer containing ascorbic acid as a stabilizer to minimize radiolysis (Figure S4a, Supporting Information).[21] However, during purification the radiolabeled nanocarriers suffered radiolytic degradation in the PD-10 size-exclusion desalting column. Thus, the purification protocols were modified by adding ascorbic acid (0.2 mg mL^{-1}) in saline while equilibrating and eluting the PD-10 column to protect the polymer nanocarriers from free radical damage.[22] As summarized in Table S1 (Supporting Information), the isolated yield and molar activities for [^{177}Lu]PEG-$(DOTA)_1$ ranged from 70.9–76.6% and 10.8–11.5 MBq nmol^{-1}, respectively. However, improved isolated yield (91.8–99.2%) and molar activity (14.6–15.8 MBq nmol^{-1}) were obtained for [^{177}Lu]PEG-$(DOTA)_1(ACUPA)_3$. PSMA-617 was also radiolabeled with ^{177}Lu following previously reported protocol,[17] that provided 90% isolated yield with a molar activity of 41.68 MBq nmol^{-1} (Figure S4b, Supporting Information).

2.2. In Vitro Cell Binding Assay

The StarPEG nanocarriers were first evaluated in vitro using PSMA+ PC3-Pip and PSMA− PC3-Flu cell lines and the PSMA targeting affinity of PEG-$(DOTA)_1(ACUPA)_3$ was compared with previously reported conjugates as positive control.

2.2.1. Competition Radioligand Binding Assay

Competitive radioligand binding was undertaken to evaluate PSMA relative binding affinity to [68Ga]PSMA-11.[23] The PSMA-2, Azido-ACUPA along with previously PET imaging analog were also evaluated as positive controls and were found to be consistent with published reports (Figure S5, Supporting Information).[24] From two independent experiments, the IC50 for the targeted nanocarrier PEG-$(DOTA)_1(ACUPA)_3$ was 1024 × 10^{-9} ± 50 × 10^{-9} M with 95% confidence interval in the range of 687 × 10^{-9}–1344 × 10^{-9} M, similar when compared to PET imaging analog PEG-$(DFB)_1(ACUPA)_3$ (637.3 × 10^{-9} M) in PSMA+ PC3-Pip cells (**Figure 2a** and Table S2, Supporting Information). As expected, no sign of any specific binding was observed in the nontargeted nanocarrier PEG-$(DOTA)_1$ (Figure 2A).

2.2.2. Saturation Binding Assay

The dissociation constants (K_d) of the 177Lu-labeled nanocarriers were calculated in PSMA+ PC3-Pip cells by saturation binding assay (Figure 2b). As summarized in Table S3 (Supporting Information), K_d of 57.5 × 10^{-9} M (95% confidence interval in the range of 52.5 × 10^{-9}–63.2 × 10^{-9} M) and B_{max} of 156 674 moles mg^{-1} protein were obtained for the targeted nanocarrier [^{177}Lu]PEG-$(DOTA)_1(ACUPA)_3$. Similar to the binding affinity observed in competition binding assay, the saturation binding assay demonstrated a similar binding affinity of the theranostic nanocarrier [^{177}Lu]PEG-$(DOTA)_1(ACUPA)_3$ as compared to its previously reported PET imaging analog [^{89}Zr]PEG-$(DFB)_1(ACUPA)_3$ (K_d = 30.96 nm) in PSMA+ PC3-Pip cells.[12] As expected, the nontargeted nanocarrier [^{177}Lu]PEG-$(DOTA)_1$ did not show any sign of specific binding in the PSMA+ PC3-Pip cells (Table S3, Supporting Information).

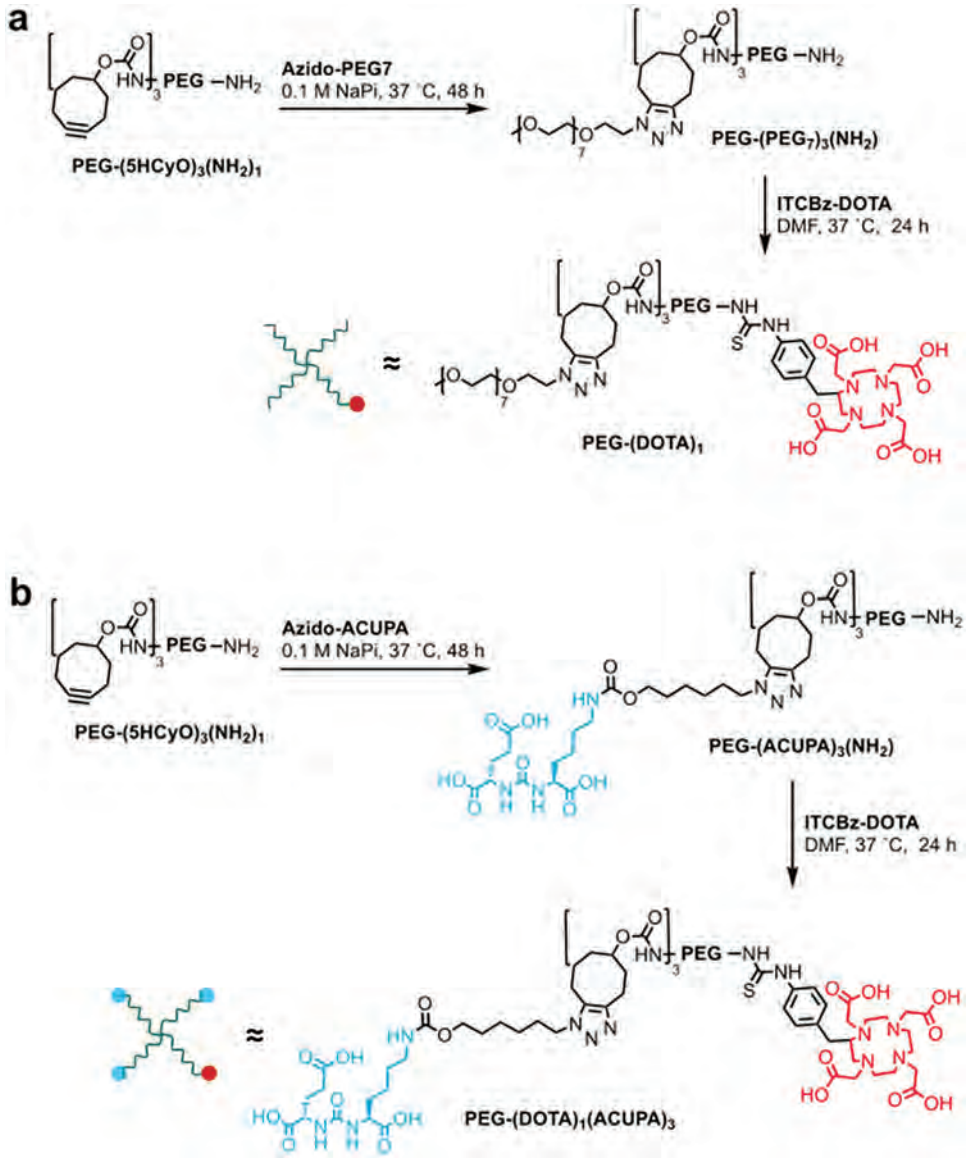

Scheme 1. Synthetic routes to the StarPEG theranostic conjugates a) PEG-$(DOTA)_1$ and b) PEG-$(DOTA)_1(ACUPA)_3$ evaluated in prostate-specific membrane antigen (PSMA)+ subcutaneous as well metastatic tumor models. Detailed synthetic protocols are provided in Experimental Section.

2.2.3. Blocking Assay

Further, the binding efficacy of both the targeted and nontargeted nanocarriers was tested in a blocking assay using PSMA-2 as the blocking agent in both PSMA+ PC3-Pip and PSMA− PC3-Flu cells (Figure 2c and Figure S6, Supporting Information). Beginning at the 1 h time point, [^{177}Lu]PEG-$(DOTA)_1(ACUPA)_3$ demonstrated high accumulation (2.77 ± 0.12% AD) in PSMA+ PC3-Pip cells, which increased up to 22.0 ± 1.16% AD at the 24 h time point. The targeted uptake of the nanocarrier was efficiently blocked >99% in the presence PSMA-2.[25] In comparison, the targeted nanocarrier in PSMA− PC3-Flu cells, along with the nontargeted nanocarrier [^{177}Lu]PEG-$(DOTA)_1$ in both PSMA+ PC3-Pip and PSMA− PC3-Flu demonstrated no sign of specific binding and the cell accumulations remained in the range of 0.04–0.06% AD.

2.2.4. Membrane-Bound and Internalization Assay

The degree of internalization of the nanocarriers was also evaluated in membrane-bound and internalization assay in both PSMA− PC3-Flu and PSMA+ PC3-Pip cells (Figure 2d and Figure S7, Supporting Information). Comparatively very high membrane-bound and internalized activities were observed for the targeted nanocarrier [^{177}Lu]PEG-$(DOTA)_1(ACUPA)_3$ in PSMA+ PC3-Pip cells. At 1 h time point, the membrane-bound activities (1.89 ± 0.11% AD) were relatively high as compared to

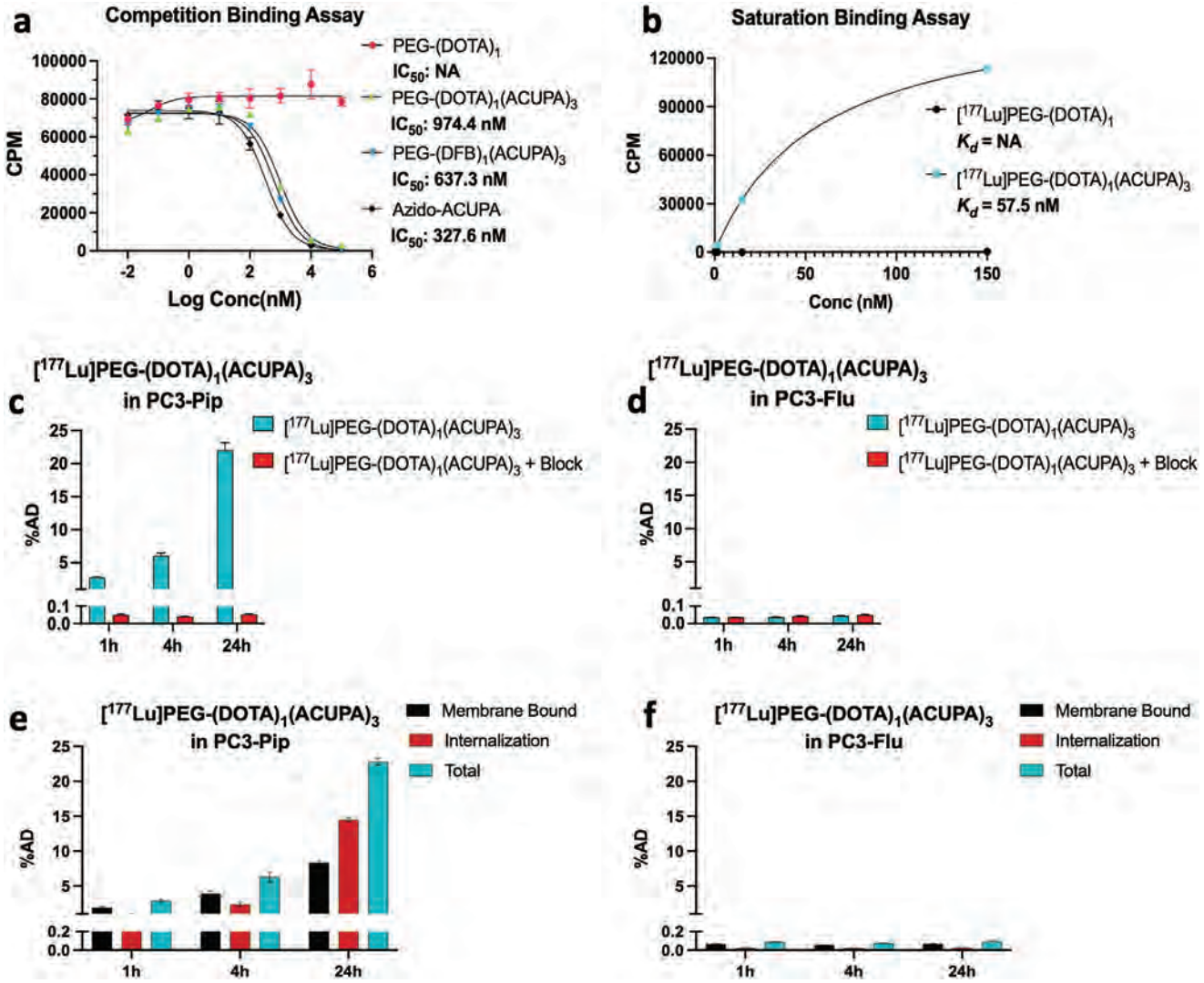

Figure 2. In vitro cell-binding assays with StarPEG nanocarriers in prostate-specific membrane antigen (PSMA)+ PC3-Pip and PSMA− PC3-Flu cell lines demonstrate efficient cell binding and uptake of PSMA-targeted theranostic agents. a) IC_{50} of nonradiolabeled theranostic StarPEGs, previously evaluated diagnostic nanocarrier PEG-(DFB)1(ACUPA)3 and azido-ACUPA determined by [^{68}Ga]PSMA-11-based in vitro competitive radioligand binding assay in PSMA+ PC3-Pip cells. b) K_d measurement of ^{177}Lu-labeled StarPEGs in the PSMA+ PC3-Pip cell line by a saturation binding assay. c,d) Blocking assay of [^{177}Lu]PEG-$(DOTA)_1(ACUPA)_3$ labeled StarPEGs (5×10^{-9} M) in PSMA+ PC3-Pip and PSMA−PC3-Flu cells using PSMA-2 (10×10^{-6} M) as the blocking agent at 1, 4, and 24 h (%AD = percentage added dose). Blocking assays with the nontargeting [^{177}Lu]PEG-$(DOTA)_1$ have been presented in Figure S6 (Supporting Information). e,f) Membrane-bound and internalization assay of the [^{177}Lu]PEG-$(DOTA)_1(ACUPA)_3$ at 1, 4, and 24 in PSMA+ PC3-Pip and PSMA− PC3-Flu cells (%AD = percentage added dose). Membrane-bound and internalization assay with the nontargeting [^{177}Lu]PEG-$(DOTA)_1$ have been presented in Figure S7 (Supporting Information). Overall, the ACUPA conjugated StarPEG nanocarrier demonstrated excellent PSMA targeted binding affinity in PSMA+ PC3-Pip cells. ($n = 3$, mean ± SD).

the internalized activities (0.95 ± 0.06% AD). However, at 24 h incubation time, the internalized activities increased significantly ($p = 0.0001$) to 14.49 ± 0.26% AD, which was 1.73 fold higher than the membrane-bound activity (8.33 ± 0.25% AD). The total activities were 2.84 ± 0.18, 6.24 ± 0.73, 22.82 ±0.49% AD at 1, 4, and 24 h, respectively and were very close to that of the bound activities obtained in blocking assay, i.e., 2.77 ± 0.12, 6.08 ± 0.37, 22.0 ± 1.16% AD at 1, 4, and 24 h, respectively (Figure 2c,d). As expected, no evidence of specific internalization or membrane binding was seen in PSMA− PC3-Flu cells and with the nontargeted nanocarrier. Overall, the in vitro cell binding results demonstrated PSMA targeted efficient cell binding and internalization of the targeted nanocarrier [^{177}Lu]PEG-$(DOTA)_1(ACUPA)_3$ in PSMA+ PC3-Pip cells.

2.2.5. Colony Formation Assay

The in vitro treatment efficacy of the targeted nanocarrier [^{177}Lu]PEG-$(DOTA)_1(ACUPA)_3$ was evaluated in both PC3-Pip and PC3-Flu cells in a colony formation assay. As presented in Figure S8 (Supporting Information), a reduction in the number

of PSMA+ PC3-Pip colonies to 38 ± 2.4% and 7 ± 1.9% was observed following treatment with 0.1 and 0.25 MBq mL^{-1} of the targeted nanocarrier, respectively. In contrast, PSMA− PC3-Flu cells remained unaffected with more than 95 ± 5.7% and 89 ± 2.0% live colonies at the same doses treatment of the nanocarrier.

2.3. In Vivo Evaluation of [^{177}Lu]PEG-$(DOTA)_1(ACUPA)_3$ in PC3-Pip and PC3-Flu Subcutaneous Dual Xenograft Models Demonstrate High PSMA Targeted Uptake In Vivo

PSMA targeted tumor accumulation of both the ^{177}Lu radiolabeled nanocarriers, [^{177}Lu]PEG-$(DOTA)_1$ and [^{177}Lu]PEG-$(DOTA)_1(ACUPA)_3$, were evaluated in the nu/nu athymic mice model with both PSMA+ PC3-Pip and PSMA− PC3-Flu tumors, which were xenografted at left and right flank, respectively (**Figure** 3a).

2.3.1. μSPECT/CT Imaging

Figure 3b shows the maximum intensity projection (MIP) and coronal view of μSPECT/CT images captured at 24 h, 72 h, 168 h and 192 h post-injection of the nanocarriers. The targeted nanocarrier, [^{177}Lu]PEG-$(DOTA)_1(ACUPA)_3$, demonstrated noticeable PSMA targeted accumulation in PSMA+ PC3-Pip tumors at 24 h post-injection. Tumor accumulation increased significantly with background clearance at 72 h onwards. Respective regions of interest (ROI) were drawn on the μSPECT images to produce time−activity curves and were in line with the observed high accumulation in μSPECT/CT images (Figure 3c,d, Table S4, Supporting Information). At 24 h post-injection, the in vivo accumulation in PC3-Pip tumors was 8.85 ± 1.17% ID cc^{-1}, which increased steadily to 22.96 ± 0.19% ID cc^{-1} at 168 h ($p = 0.0035$). Interestingly, previously reported 89Zr-labeled PET analogs of the StarPEG nanocarriers showed maximum PC3-Pip accumulation at 72 h post-injection, followed by a steady decrease in tumor activity retention. However, the theranostic StarPEG nanocarrier tagged with ^{177}Lu-DOTA demonstrated very stable and long-term tumor retention at 23.47 ± 0.94% ID cc^{-1} after 192 h post-injection, which is highly desirable for better treatment. The blood pool activity decreased drastically from 14.32 ± 0.24% ID cc^{-1} at 24 h to 1.99 ± 0.08% ID cc^{-1} at 192 h post-injection (Figure S9, Supporting Information). Significant uptake was noted in the skin and subcutaneous tissues, similar to our prior report utilizing 89Zr labeled nanocarriers.[12] In comparison, the targeted nanocarrier in PSMA− PC3-Flu tumors and the nontargeted nanocarrier in both PC3-Pip and PC3-Flu tumors demonstrated around 5% ID cc^{-1} accumulation without any noticeable SPECT signal in the tumors.

2.3.2. Ex Vivo Organ Biodistribution

As schematically demonstrated in Figure 3a, three mice injected with 9–10 MBq from each group were sacrificed at 72 and 192 h post-injection to collect the major organs and the distribution of the ^{177}Lu-labeled nanocarriers was quantified in a gamma counter. All the ex vivo organ biodistribution results are summarized in **Figures** 4a–e and S10 and Tables S5–S8 (Supporting Information). The targeted nanocarrier [^{177}Lu]PEG-$(DOTA)_1(ACUPA)_3$ showed high specific accumulation of 21.3 ± 1.57 and 21.3 ± 8.8% ID g^{-1} in PSMA+ PC3-Pip tumors at 72 and 192 h, respectively. In comparison, the targeted nanocarrier demonstrated 4.7 ± 0.11% ID g^{-1} accumulation in PSMA− PC3-Flu tumors that decreased to 3.1 ± 0.39% ID g^{-1} at 192 h post-injection. Similarly, the nontargeted nanocarrier [^{177}Lu]PEG-$(DOTA)_1$ demonstrated 6.2 ± 2.26 and 7.0 ± 1.02% ID g^{-1} uptake in PC3-Pip and PC3-Flu tumors at 72 h and decreased to 3.6 ± 0.73 and 4.6 ± 1.06% ID g^{-1} at 192 h post-injection, respectively. Overall, the nanocarrier with three copies of ACUPA ligands demonstrated very high PSMA targeted accumulation in PSMA+ PC3-Pip xenografts with excellent PC3-Pip tumor to muscle ratio (25.5 at 72 h and 13.7 at 192 h), PC3-Pip tumor to blood ratio (3.5 at 72 h and 20.4 at 192 h) and PC3-Pip tumor to PC3-Flu tumor ratio (4.5 at 72 h and 6.9 at 192 h). Additionally, the PSMA-targeted nanocarrier showed around 12.4% ID g^{-1} accumulation in the kidney at 72 h that remained stable at 192 h post-injection, whereas the nonspecific nanocarrier demonstrated low kidney uptake, 1.78 and 0.97% ID g^{-1} at 72 and 192 h, respectively. Mouse kidneys are well-known to bear elevated PSMA expression.[26] Collectively, these results confirm the high specificity of the targeted StarPEG nanocarrier.

2.3.3. Autoradiography and Histology Analysis

Major organs harvested during the biodistribution experiments were studied with autoradiographic and histologic analysis to explore the tumor penetration. **Figures** 5a and S11 (Supporting Information) demonstrate elevated radiopharmaceutical accumulation in PSMA+ PC3-Pip tumors treated with the targeted nanocarrier [^{177}Lu]PEG-$(DOTA)_1(ACUPA)_3$. In comparison, the targeted nanocarriers in PSMA− PC3-Flu xenografts and the nontargeted nanocarrier in both the PC3-Pip and PC3-Flu tumors showed very faint peripheral intensity that markedly decreases from days 3 to 8. Despite very high PC3-Pip tumor accumulation of the targeted nanocarrier in PC3-Pip tumors compared to PC3-Flu, the bulk of the activity was observed around the tumor periphery. Tumor slices were stained with hematoxylin and eosin (H&E) (Figure S12, Supporting Information) to correlate with tumor distribution, demonstrating largely homogeneous tumor cellularity with a few small areas of necrosis. Overall, these studies demonstrated that the targeted nanocarrier demonstrated significantly elevated tissue penetration in PC3-Pip xenografts.

2.3.4. Absorbed Dose Calculation

Both tumor and normal tissue dosimetry were performed by drawing volumes of interest (VOIs) on coregistered CT images in μSPECT/CT data of the subcutaneous tumor-bearing mice model. It should be noted that the mice were injected with 38.4–43.2 MBq ^{177}Lu-labeled nanocarriers for better μSPECT/CT imaging, but all the mice died on day 10 post-injection due to high activity. Because of the high dose injection, all the tumors received a high therapeutic absorbed dose (793.8 ± 167.2 mSv MBq^{-1}) irrespective of nanocarriers and tumor model (Table S9,

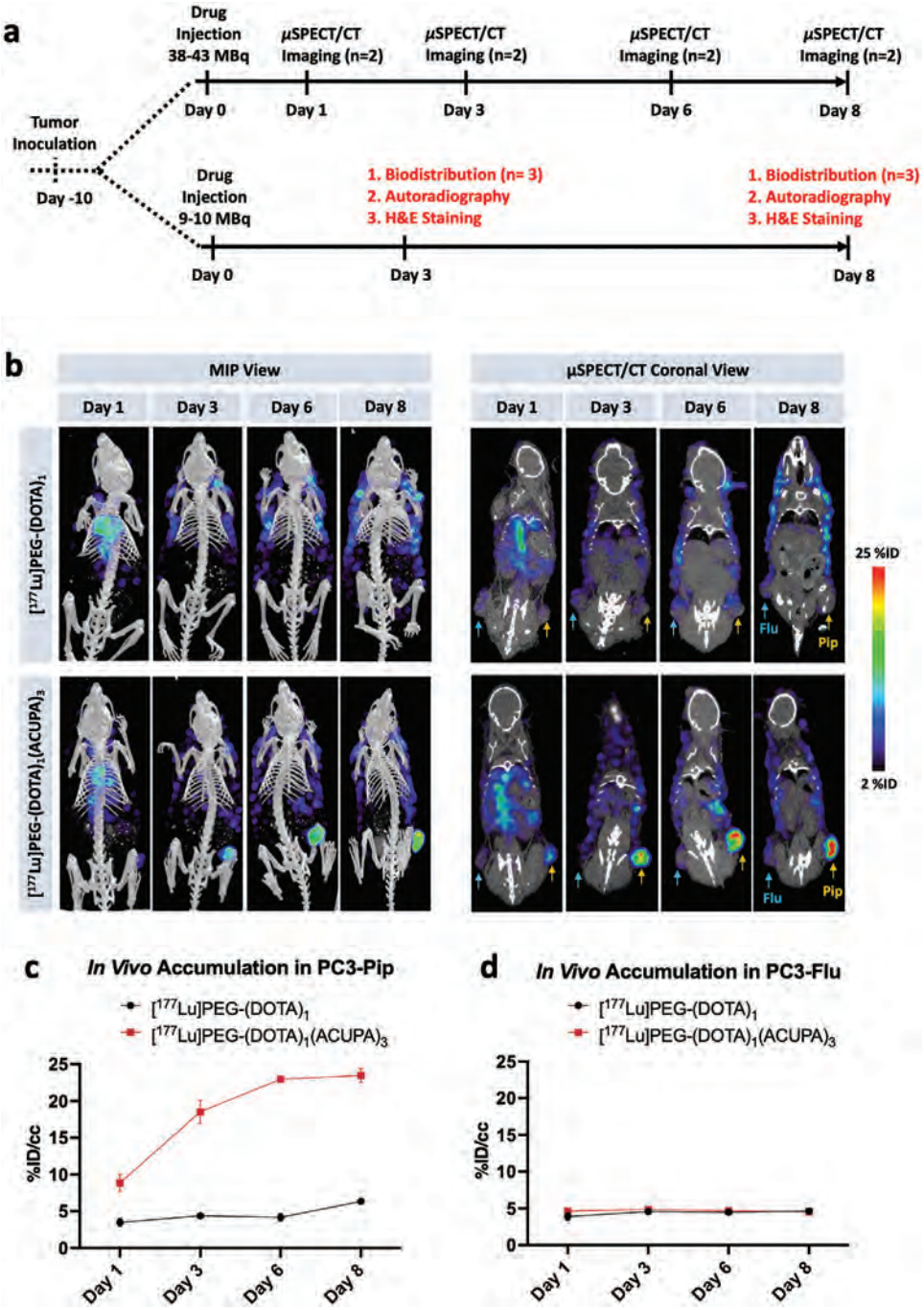

Figure 3. In vivo μSPECT (micro single-photon emission computed tomography)/CT imaging demonstrates prostate-specific membrane antigen (PSMA) targeted accumulation of StarPEG nanocarriers in PSMA+ PC3-Pip subcutaneous tumors. a) Representation of experimental design for in vivo evaluation of the ^{177}Lu-labeled StarPEGs in mice bearing dual xenografts of PSMA+ PC3-Pip (left flank) and PSMA− PC3-Flu (right flank). b) Maximum intensity projection (MIP) μSPECT/CT and coronal μSPECT/CT images obtained on days 24, 72, 144, and 192 h post-injection of ^{177}Lu-labeled StarPEGs reveal high tumor accumulation of targeted nanocarriers in PSMA+ PC3-Pip. c,d) Quantification of in vivo tumors' accumulation by drawing regions of interest (ROIs) on the respective tumors at 24, 72, 144, and 192 h post-injection of ^{177}Lu-labeled StarPEGs. ROIs on the heart at respective imaging time points are presented in Figure S9 (Supporting Information). Overall, the in vivo μSPECT/CT imaging demonstrated excellent PSMA targeted tumor accumulation of the ACUPA conjugated StarPEG nanocarrier in PSMA+ PC3-Pip xenografts. ($n = 2$, mean ± SD).

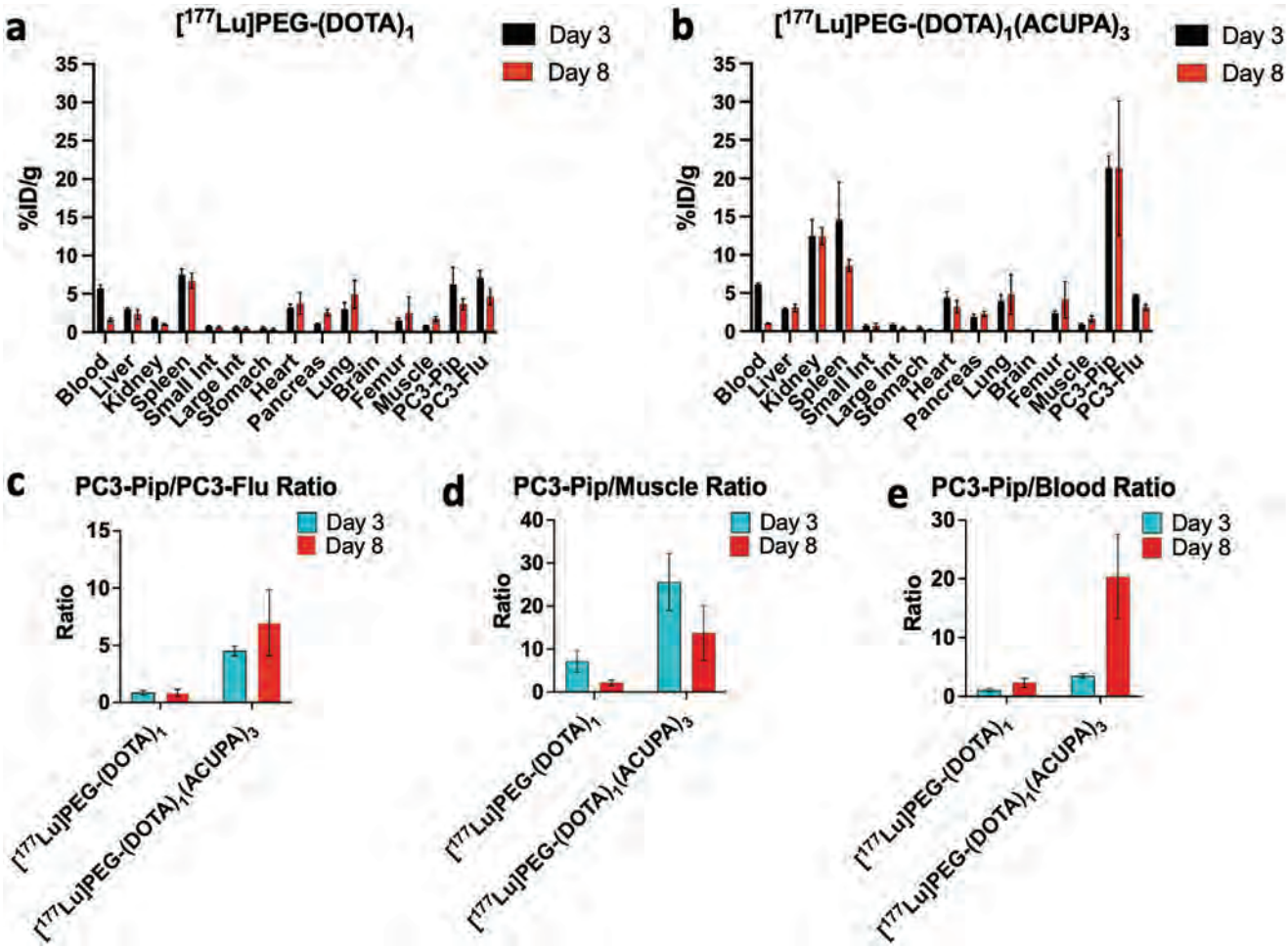

Figure 4. Ex vivo organ biodistribution of ^{177}Lu-labeled StarPEG nanocarriers. Organ biodistribution of a) [^{177}Lu]PEG-(DOTA)1 and b) [^{177}Lu]PEG-$(DOTA)_1(ACUPA)_3$ at 72 and 192 h post-injection of the nanocarriers ($n = 3$, mean ± SD). The ratio of c) PC3-Pip to PC3-Flu, d) PC3-Pip to the muscle, and e) PC3-Pip to the blood of [^{177}Lu]StarPEGs at 72 and 192 h post-injection of the nanocarriers ($n = 3$, mean ± SD). The Supporting Information presents ex vivo organ biodistribution of [^{177}Lu]StarPEGs in % ID/Organ (Figure S10, Supporting Information). Overall, the ex vivo organ biodistribution demonstrated excellent prostate-specific membrane antigen (PSMA) targeted tumor accumulation of the ACUPA conjugated StarPEG nanocarrier in PSMA+ PC3-Pip xenografts.

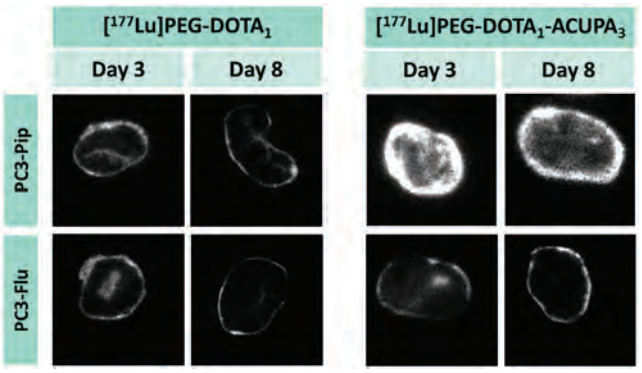

Figure 5. Autoradiography images of 20 µm tumor slices of prostate-specific membrane antigen (PSMA)+ PC3-Pip and PSMA− PC3-Flu tumors collected after 72 and 192 h post-injection of [^{177}Lu]StarPEG nanocarriers. Overall, the targeted nanocarrier demonstrated superior tissue penetration in PSMA+ PC3-Pip xenografts.

Supporting Information).[27] However, the targeted nanocarrier [^{177}Lu]PEG-$(DOTA)_1(ACUPA)_3$ demonstrated more than 5.2-fold higher absorbed dose (4155 ± 209.3 mSv MBq^{-1}) in PSMA+ PC3-Pip tumors compared to PC3-Flu suggesting highly potent targeted antitumor dosing. The percent injected activity (%IA) within the defined organs was extrapolated to human-equivalent organ and whole-body effective doses using ratios of standard human organ weights to mouse organ weights. Tables S10 and S11 (Supporting Information) summarized the organ and effective dose estimated using OLINDA version 1.1 with ICRP Publication 60 tissue weighting factors. The normal tissue dose estimation demonstrated noticeable lungs and liver retention with washout over time. The normal tissue dosimetry suggested that the lungs are at the highest risk for radiation exposure (≈1 mSv MBq^{-1}). At the same time, other major organs, including the liver, kidneys and heart, demonstrated below 0.5 mSv MBq^{-1} absorbed doses.

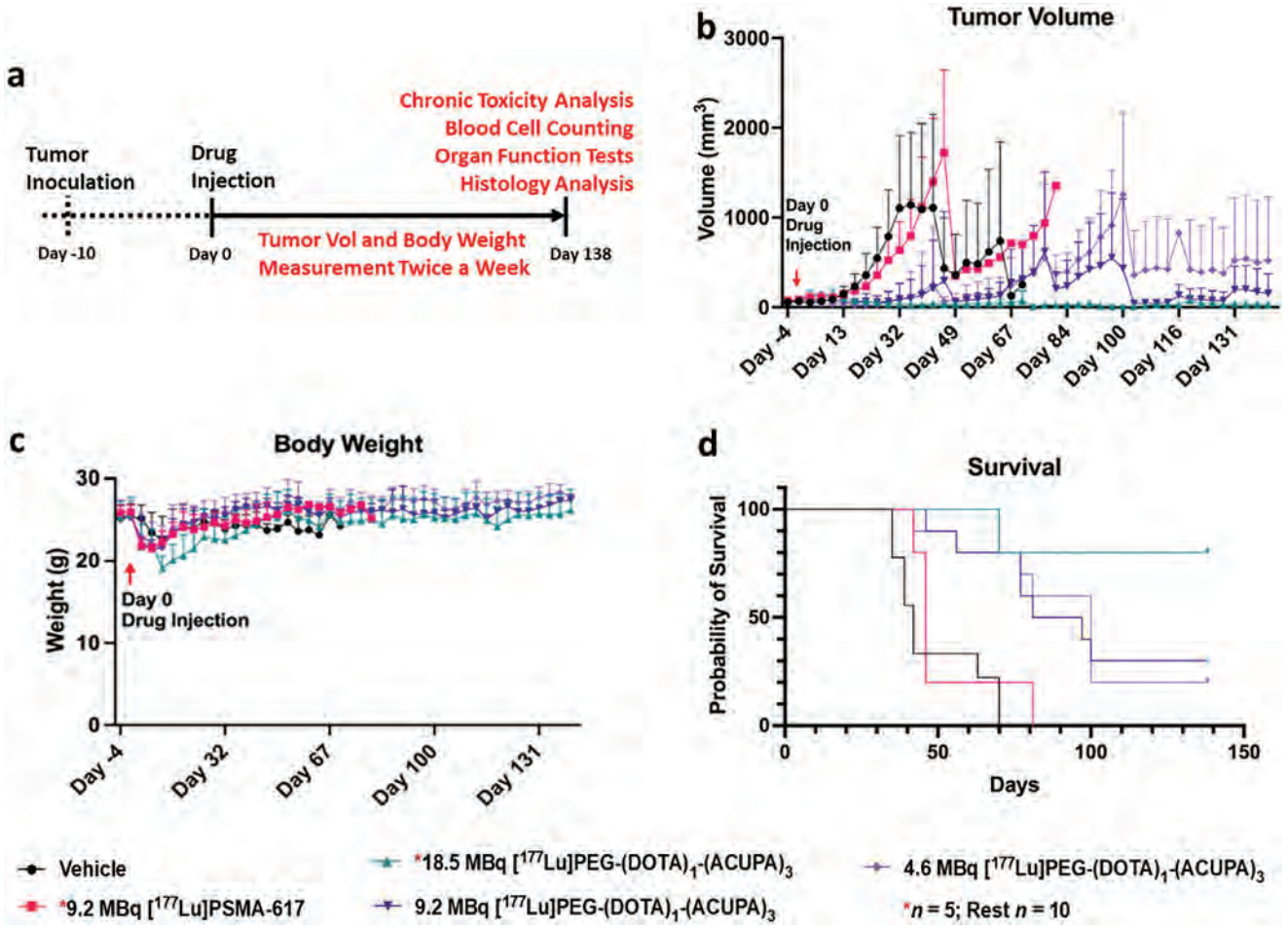

Figure 6. In vivo treatment study of [^{177}Lu]PEG-(DOTA)$_1$(ACUPA)$_3$ in nude mice models bearing prostate-specific membrane antigen (PSMA)+ PC3-Pip tumors. a) Representation of experimental design for in vivo treatment efficacy and toxicity of ^{177}Lu-labeled StarPEGs in mice models bearing PSMA+ PC3-Pip subcutaneous tumors. Tumor volume (b), body weight (c), and survival (d) of mice models bearing PC3-Pip tumors and treated with different doses (0, 4.6, 9.2, and 18.5 MBq) of either [^{177}Lu]PEG-(DOTA)$_1$(ACUPA)$_3$ or 9.2 MBq of [^{177}Lu]PSMA-617. Overall, a single 18.5 MBq dose of [^{177}Lu]PEG-(DOTA)$_1$(ACUPA)$_3$ demonstrated highly efficient suppression of the tumor volume without any regrowth of tumors with 80% survival at 138 days post-drug injection. (n = 10, mean ± SD).

2.4. Treatment Studies with [^{177}Lu]PEG-(DOTA)$_1$(ACUPA)$_3$

As observed in the in vivo evaluation in the mice models bearing subcutaneous dual xenografts, the PSMA targeted nanocarrier demonstrated high specificity toward PSMA+ PC3-Pip tumors with around fivefold higher absorbed dose compared to the nontargeted nanocarrier and the PSMA− PC3-Flu tumors. This encouraged us to evaluate therapeutic potential of the 177Lu labeled targeted nanocarrier in subcutaneous as well as metastatic tumor-bearing mice models. As observed in the dosimetry analysis, 38.4–43.2 MBq dose demonstrated high radiation exposure and toxicity to the normal tissue. Thus, the mice were treated with 18.5 MBq or less for the therapy study.

2.4.1. Treatment Studies in PSMA+ PC3-Pip Subcutaneous Models

As demonstrated in **Figure** 6a, after 10 days of cell inoculation, the mice with PC3-Pip subcutaneous tumors of 100–200 mm3 were treated with the targeted nanocarrier [^{177}Lu]PEG-(DOTA)$_1$(ACUPA)$_3$ and the tumor volume and bodyweight of the mice were monitored. Along with the injection of different doses (18.5, 9.2, and 4.6 MBq) of the targeted nanocarrier, one cohort of mice (n = 5) was treated with 9.2 MBq of [^{177}Lu]PSMA-617 as a positive control.[28] Figure 6b–d shows the tumor volume, body weight, and survival of the mice up to 138 days post-treatment of the drugs. A single 18.5 MBq dose of [^{177}Lu]PEG-(DOTA)$_1$(ACUPA)$_3$ demonstrated highly efficient suppression of the tumor volume without any regrowth of tumors with 80% survival at 138 days post-drug injection. Both 9.2 and 4.6 MBq doses of [^{177}Lu]PEG-(DOTA)$_1$(ACUPA)$_3$ significantly delayed the tumor growth compared to the vehicle and 9.2 MBq single dose of [^{177}Lu]PSMA-617. The median survival of 9.2 and 4.6 MBq doses of [^{177}Lu]PEG-(DOTA)$_1$(ACUPA)$_3$ were 89 and 100 days, respectively. However, the tumor growth pattern in mice injected with a vehicle and 9.2 MBq single doses of [^{177}Lu]PSMA-617 were similar, with 42 and 46 days of median survival, respectively. Post-drug treatment, a sharp body weight loss was witnessed in al-

most all mice, including the negative control mice. This was determined to be due to *Corynebacterium* Bovis bacterial infection (Figure 6c).[29] After treatment with antiseptic chlorhexidine, the mice recovered weight within 2–3 weeks.[29]

2.4.2. Chronic Toxicity Studies in PC3-Pip Subcutaneous Models

As schematically presented in Figure 6a, the therapy experiment ended 138 days post-drug injection and the mice that survived were euthanized for chronic toxicity analysis, which included four mice at the 18.5 MBq dose, two mice at the 9.2 MBq dose, and three mice at the 4.6 MBq dose. Additionally, three untreated healthy mice were included in the toxicity analysis as control. Laboratory analyses for kidney function tests revealed elevated blood urea nitrogen levels in the 18.5 and 9.2 MBq dose levels, but normal creatinine, suggesting mild to moderate renal toxicity (Figure S13, Tables S12 and S13, Supporting Information). Additionally, elevated alkaline phosphatase levels were observed in the 4.6 and 18.5 MBq treatment groups, indicating possible liver toxicity (Figure S13, Supporting Information). Importantly, all other liver parameters remained unchanged. Histologic analysis further confirmed the toxicity seen in organ function tests. Histological features of most major organs appeared normal at all three doses, including the heart, lung, bone marrow, and spleen tissue (Figure S14, Supporting Information). Kidney parenchyma revealed mild kidney injury at the 4.6 MBq dose, moderate injury at the 9.2 MBq dose, and moderate to marked injury at the 18.5 MBq dose (Figure S13c, Supporting Information). The kidney injury consisted predominantly of increased glomerular fibrin deposition, reduced capillaries in glomeruli and cortical tubule atrophy. The liver tissue also appeared normal, except centrizonal inflammation was observed in one mouse with 9.2 MBq dose of [^{177}Lu]PEG-(DOTA)$_1$(ACUPA)$_3$.

2.4.3. Treatment Studies in PC3-Pip Metastatic Models Monitored by [^{68}Ga]PSMA-11 μPET/CT Imaging

The treatment efficacy of the targeted nanocarrier [^{177}Lu]PEG-(DOTA)$_1$(ACUPA)$_3$ was further evaluated in mice bearing PC3-Pip metastatic tumors developed by the inoculation of PC3-Pip cells in the left ventricle of the heart by intracardiac injection. As depicted in the experimental protocol (**Figure 7a**), two cohorts of mice (n = 10) were injected with either vehicle or 9.2 MBq of [^{177}Lu]PEG-(DOTA)$_1$(ACUPA)$_3$ after 10 days of cell injection. The treatment efficacy of the nanocarrier was monitored by [^{68}Ga]PSMA-11 based μPET/CT imaging, body weight measurement and organ biodistribution. The mice were subjected to [^{68}Ga]PSMA-11 μPET/CT imaging 1 day before, on days 18 and 35 of drug treatment (^{177}Lu labeled nanocarrier) (Figure 7b). The control mice without drug treatment developed metastatic tumors in the neck region, demonstrating strong accumulation of [^{68}Ga]PSMA-11. However, no such metastatic tumors were observed in the treated group with 100% survival up to 51 days, indicating efficient metastatic tumor growth suppression without significant body weight loss (Figure 7c). Importantly, the overall survival was markedly improved in the treatment group compared against the control (Figure 7d). A small cohort of three mice from each group were subjected to organ biodistribution on days 35 and 51 post-drug injection. As shown in Figure 7e–f, Figures S15 and S16 and Tables S14–S17 (Supporting Information), a relatively high accumulation of [^{68}Ga]PSMA-11 was observed in most of the major organs, including liver metastases, in the control group as compared to the drug-treated group indicating the burden of metastatic tumor in those organs. Overall, this experiment demonstrates that [^{177}Lu]PEG-(DOTA)$_1$(ACUPA)$_3$ was effective in eliminating metastatic prostate cancer in the PC3-PiP model.

3. Discussion

Herein, the current study has evaluated the PSMA-targeted in vitro binding efficacy along with in vivo SPECT imaging and therapeutic potential of newly synthesized 4-armed StarPEG nanocarriers (40 kDa MW) conjugated with three copies of PSMA targeting ACUPA ligands (Figure 1). Most of the prostate cancer tumor models evaluated with large size nanocarriers have been reported to be EPR low phenotype and demonstrate heterogeneous low tumor uptake and tissue penetration of nanocarriers due to their poor vascular development.[12,14] However, our prior finding demonstrated significant improvement in the delivery and tissue penetration of StarPEG nanocarriers in PSMA+ PC3-Pip tumors with long-term tumor retention after conjugating PSMA-targeting ACUPA ligands, which is highly desirable for better therapeutic efficacy.[12] Therefore, the diagnostic radiometal-chelator pair ^{89}Zr-DFB was replaced with ^{177}Lu-DOTA for radiopharmaceutical therapy. As presented in Figure 1 and Scheme 1, two StarPEG nanocarriers were synthesized, PSMA-targeted PEG-(DOTA)$_1$(ACUPA)$_3$ and nontargeted PEG-(DOTA)$_1$, for comparative evaluation of PSMA-targeted SPECT imaging and treatment studies in both subcutaneous as well as metastatic tumor models.

The designed StarPEG conjugates were successfully synthesized and radiolabeled with ^{177}Lu in good yields (Scheme 1).[6,12,21] Initially, despite efficient radiolabeling, the isolated labeled nanocarrier yield was below 10%, especially in scale-up radiosynthesis. Surprisingly, a major fraction of the activity was retained in the stationary phase of PD-10 size-exclusion desalting column, indicating radiolytic degradation of the StarPEG nanocarriers. To restrict the free radical damage and stabilize the radiolabeled nanocarriers, the antioxidant ascorbic acid containing was used in the saline solution while equilibrating and eluting the polymer nanocarriers.[22] This minor modification in the purification protocol resulted in excellent radiochemical yield (Table S1, Supporting Information) and [^{177}Lu]PEG-(DOTA)$_1$(ACUPA)$_3$ stability. The molar activity for [^{177}Lu]PEG-(DOTA)$_1$ was 10.8–11.9 MBq nmol^{-1}. A slight improvement in molar activity (14.6–15.8 MBq nmol^{-1}) was noted for [^{177}Lu]PEG-(DOTA)$_1$(ACUPA)$_3$. Overall, two StarPEG nanocarriers with or without three copies of PSMA targeting ACUPA ligands were synthesized and radiolabeled with ^{177}Lu with suitable molar activities for imaging and therapy.

Multiple time points in vivo μSPECT/CT imaging and ex vivo organ biodistribution demonstrated that, unlike the previously reported diagnostic StarPEG nanocarrier [^{89}Zr]PEG-(DFB)$_1$(ACUPA)$_3$,[12] no partial tumor clearance of the theranostic nanocarrier was observed after 72 to 192 h post-injection

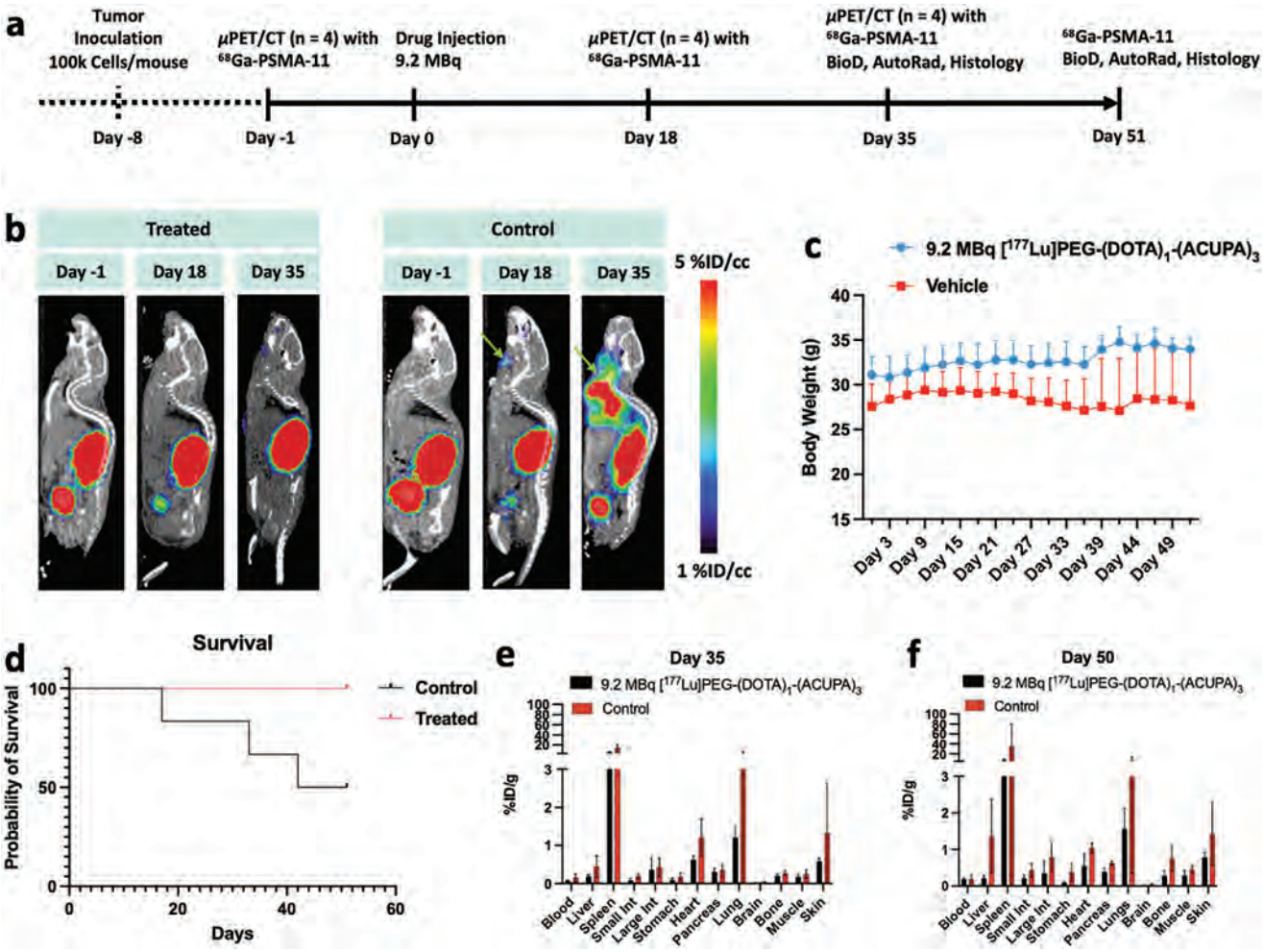

Figure 7. [^{177}Lu]PEG-(DOTA)$_1$(ACUPA)$_3$ was effective in suppressing the growth of metastatic prostate cancer in the PC3-PiP intracardiac metastatic model. a) Representation of experimental design for in vivo treatment study of the ^{177}Lu-labeled StarPEGs in mice bearing prostate-specific membrane antigen (PSMA)+ PC3-Pip metastatic tumors. b) Multiple time points [^{68}Ga]PSMA-11 μPET/CT imaging of the nude mice bearing PC3-Pip metastatic tumors before and after treatment of 9.2 MBq [^{177}Lu]PEG-(DOTA)$_1$(ACUPA)$_3$ (n = 4, mean ± SD). c) Body weight measurement of the treated and control mice up to 51 days post-injection of 9.2 MBq [^{177}Lu]PEG-(DOTA)$_1$(ACUPA)$_3$. d) Overall survival of mice models bearing PC3-Pip metastatic tumors and treated with/without 9.2 MBq) of [^{177}Lu]PEG-(DOTA)$_1$(ACUPA)$_3$. e,f) [^{68}Ga]PSMA-11 organ biodistribution of the nude mice bearing PC3-Pip metastatic tumors on 35 and 50 days post-treatment of 9.2 MBq [^{177}Lu]PEG-(DOTA)$_1$(ACUPA)$_3$ (n = 10, mean ± SD). Overall, a single 9.2 MBq dose of [^{177}Lu]PEG-(DOTA)$_1$(ACUPA)$_3$ demonstrated highly efficient suppression of PC3-Pip metastatic tumors with 100% survival at 51 days post-drug injection.

(Figures 3–4). In fact, the highest PC3-Pip to blood ratio of 20.4 was witnessed at 192 h, which was highly desirable and could potentially enhance the therapeutic efficacy of the nanocarrier. In comparison, the targeted nanocarrier in PSMA− PC3-Flu tumors and the nontargeted nanocarrier in both PC3-Pip and PC3-Flu tumors demonstrated around 5% ID cc^{-1} passive accumulation without any noticeable SPECT signal in the tumors. Such low nontargeted tumor accumulation could be the EPR-mediated passive uptake of the nanocarriers and was in line with previously reported nontargeted StarPEG nanocarriers.[12] Besides, the PSMA-targeted nanocarrier showed a high accumulation in the kidney compared to that of the nontargeted nanocarrier, which further confirmed the specificity of the developed StarPEG nanocarrier considering the fact that mouse kidney is also well known to bear elevated PSMA expression (Figure 4b).[26] Despite excellent PSMA targeting affinity, the targeted nanocarrier demonstrated heterogenous peripheral accumulation in PC3-Pip tumors as observed in the high-resolution autoradiography images, which may be due to the poor vascularity of this prostate xenograft.[7,9]

Tumor and whole-body dosimetry analysis of the nanocarriers was performed by drawing VOIs in μSPECT/CT images (Table S9, Supporting Information). Since the mice were injected with a dose above 37 MBq for better SPECT image resolution, all the tumors received a high therapeutic absorbed dose (29.3 ± 6.18 Gy, 793.8 ± 167.2 mSv MBq^{-1}) irrespective of nanocarriers and tumor model.[19,27] Importantly, the tumor dosimetry results demonstrated more than 5.2-fold higher dose delivery (153.7 ± 7.74 Gy, 4155 ± 209.3 mSv MBq^{-1}) in PC3-Pip compared to PC3-Flu. One potential limitation of our dosimetry data was that the

SPECT imaging was performed at higher administered activity of the radiopharmaceutical compared to the treatment studies. It has been observed that patients receiving as low as 14 Gy tumor-absorbed doses of [^{177}Lu]PSMA-617 demonstrated more than 50% reduction of prostate-specific antigen.[19] This suggests that the PSMA-targeted nanocarrier could have a considerable therapeutic efficacy at as low as 3.36 MBq dose in PSMA+ Pc3-Pip tumors. Calculation of human-equivalent organ and whole-body effective doses demonstrated the highest risk of lung radiation exposure, mostly around 1 mSv MBq^{-1}. However the histology analysis of the mice 138 days post-treatment of up to 9.2 MBq of [^{177}Lu]PEG-$(DOTA)_1(ACUPA)_3$ showed no sign of toxicity (Figure S14, Supporting Information).

Considering the very high toxicity of the 37 MBq dose, the mouse models bearing PC3-Pip xenografts were subjected to therapy with three different single-dose treatments (18.5, 9.2, and 4.6 MBq) of [^{177}Lu]PEG-$(DOTA)_1(ACUPA)_3$ (Figure 6) and saline solution containing ascorbic acid as a vehicle control. Interestingly, as low as a single dose of 4.6 MBq significantly delayed the tumor growth (100 days median survival) compared to the vehicle (42 days). Highly efficient antitumor response was observed in 18.5 MBq dose of [^{177}Lu]PEG-$(DOTA)_1(ACUPA)_3$ without any regrowth of tumor up to 138 days. The single dose antitumor response of 9.2 MBq [^{177}Lu]PSMA-617 (46 days median survival) was consistent with prior literature (51 days median survival) in the same animal model.[28] In contrast, our vehicle group demonstrated noticeable delayed tumor growth with 42 days of median survival compared to prior literature.[28]

Apart from the subcutaneous models, the therapeutic efficacy of the targeted nanocarrier was also evaluated in PC3-Pip metastatic tumor models by monitoring with [^{68}Ga]PSMA-11 based μPET/CT imaging. A single dose of 9.2 MBq [^{177}Lu]PEG-$(DOTA)_1(ACUPA)_3$ demonstrated efficient antitumor response with no sign of any metastatic tumor up to 51 days, while the control mice without any drug treatment developed metastatic tumors in the neck region and reduced overall survival (Figure 7b,d). Additionally, the organ biodistribution on days 35 and 51 demonstrated suppression of tumor burden of major organs, including liver, lungs, and spleen in [^{177}Lu]PEG-$(DOTA)_1(ACUPA)_3$ treated group as compared to the control group.

As observed in the imaging experiment, doses above 37 MBq dose were extremely radiotoxic for the mice and all mice died on day 10 post-injection of the nanocarriers with rapid weight loss. However, none of the mice in the therapy cohort, treated with 18.5 MBq of [^{177}Lu]PEG-$(DOTA)_1(ACUPA)_3$ or less, reached the endpoint as a result of weight loss. The long lived nature of the nanocarriers results in a higher systemic radiation dose, and potentially greater toxicity compared to small molecule counterparts. Temporary body weight loss was observed in all the cohorts post-drug injection due to *Corynebacterium bovis* bacterial infection (Figure 6c).[29] However, the mice recovered body weight quickly after treatment with antiseptic chlorhexidine.[29] Although the nanocarriers follow a hepatic clearance path, no marked histologic evidence of liver damage was observed. Among most of the major organs, only kidneys demonstrated prominent dose-dependent toxicity in both the histology and laboratory analysis (Figure S13c, Supporting Information). This could be due to the elevated PSMA expression in the mouse kidneys,[26] resulting in higher accumulation of the targeted nanocarriers in the kidneys, as observed in the ex vivo biodistribution (Figure 4b). However, the kidney toxicity observed for the nanocarrier might not be a major concern for clinical translation since the PSMA expression in human kidneys is significantly lower than that of mouse kidneys.[26] Alternate approaches to mitigate kidney toxicity could include dose reduction or fractionation.

Overall, the excellent antitumor response of [^{177}Lu]PEG-$(DOTA)_1(ACUPA)_3$ demonstrates strong feasibility of clinical translation. Single-dose treatment of the StarPEG nanocarrier with three PSMA-targeting ligands demonstrated significant improvement in tumor growth suppression and mice survival. Our approach has some similarities to prior work incorporating albumin-binding ligands in small molecule binding agents, which substantially increases serum half-life, now being investigated in clinical trials.[30] A major limitation of this work was the single time point chronic toxicity analysis with relatively small cohort size. Future analysis needs to include multiple time points for both acute and chronic toxicity studies. There are several future directions for further optimizations and improvements. Apart from the dose reduction and/or fractionation, studying alternate therapeutic isotopes such as ^{225}Ac or ^{212}Pb may be advantageous.[31] As the size and conformation of the nanocarriers may significantly influence tumor accumulation, further optimization of size and valency may be beneficial to improve the therapeutic efficacy of the StarPEG nanocarriers.

4. Conclusion

In conclusion, a PSMA-targeted StarPEG theranostic nanocarrier, [^{177}Lu]PEG-$(DOTA)_1(ACUPA)_3$, has been designed and synthesized for imaging and therapy of prostate cancer, which demonstrated excellent suppression of both subcutaneous and metastatic PSMA+ PC3-Pip xenografts. The single-dose therapeutic efficacy of the nanocarrier was compared to that of [^{177}Lu]PSMA-617, which demonstrated significant improvement in the therapeutic efficacy of [^{177}Lu]PEG-$(DOTA)_1(ACUPA)_3$ in preclinical models affirming potential clinical future translation.

5. Experimental Section

Materials and Instrumentation: The 4-armed PEG_{40kDa}-$(NH_2)_4$ was purchased from SINOPEG (Fujian, China). $^{177}LuCl_4$ was procured from MU Research Reactor (MURR) University of Missouri (Columbia, MO; US DOE Isotope Program) and p-SCN-Bn-DOTA from Macrocyclics (Plano, TX). RPMI-1640 media, penicillin–streptomycin (P/S) solutions, and fetal bovine serum (FBS), were purchased from Life Technologies (Carlsbad, CA) and Thermo Fisher Scientific (Waltham, MA). Other chemicals (solvents, reagents, and building blocks) were bought from Thermo Fisher Scientific, VWR, or Sigma Aldrich and used without further processing. ^{1}H NMR spectra were recorded in a Bruker 400 MHz NMR, respectively. Chemical shifts were shown in parts per million (ppm, δ). Transmission electron microscope images were recorded in a JEOL JEM-1230 TEM instrument.

General Synthesis of StarPEG Conjugates: HPLC was performed using a 4.6 × 150 mm 5 μm 300 Å Phenomenex Jupiter C18 reversed-phase column with a 15-min linear gradient of 0–100% acetonitrile/water/0.1% trifluoroacetic acid (TFA) (1.0 mL min^{-1}) beginning 2 min after injection unless otherwise mentioned. The starting materials and linkers including

PEG-$(5HCyO)_3(NH_2)_1$, Azido-PEG_7, and Azido-ACUPA were synthesized following the previously reported procedure.[15]

Synthesis of PEG-$(PEG_7)_3(NH_2)$ and PEG-$(ACUPA)_3(NH_2)$: PEG-$(5HCyO)_3(NH_2)$ (200 mg, 5 µmol) was dissolved in 1 mL of 0.1 M sodium phosphate (pH 7.4) and treated with either a 25×10^{-3} M solution of Azido-ACUPA (1.0 mL, 25 µmol, 1.7 Eq) or Azido-PEG_7 (9 mg, 10 µL, 22.5 µmol, 1.5 Eq) in 0.1 M sodium phosphate, pH 7.4, for 48 h at 37 °C, then dialyzed (SpectraPor 2 membrane, 12–14 kDa cutoff) against water followed by methanol and dried under reduced pressure to afford the respective intermediates, PEG-$(PEG_7)_3(NH_2)$ (Yield 75%, 150 mg) and PEG-$(ACUPA)_3(NH_2)$ (Yield 88%, 175 mg).

Synthesis of PEG-$(DOTA)_1$ and PEG-$(DOTA)_1(ACUPA)_3$: A solution of the respective intermediates, PEG-$(PEG_7)_3(NH_2)$ (97 mg, 2.4 µmol) and PEG- $(ACUPA)_3(NH_2)$ (164 mg, 4.1 µmol), in DMF (1.0 mL) was mixed with a 10 mg mL^{-1} solution of p-isothiocyanatobenzyl-DOTA (p-SCN-Bn-DOTA) in DMSO (Macrocyclics, 1.5 Eq) and *N*,*N*-diisopropylethylamine (10 Eq) in separate reaction vials and kept at 37 °C for 24 h. The mixtures were dialyzed against water (SpectraPor 2 membrane, 12–14 kDa cutoff) to remove unconjugated materials, followed by methanol and dried under reduced pressure to provide the product PEG-$(DOTA)_1$ (yield 93%, 90 mg) and PEG-$(DOTA)_1(ACUPA)_3$ (yield 91%, 150 mg). ^{1}H NMR is provided in the Supporting Information.

Cell Culture: Unless otherwise specified, the PSMA– PC3-Flu and PSMA+ PC3-Pip cell lines were cultured in RPMI1640 medium containing 10% FBS and 1% penicillin/streptomycin (P/S) at 37 °C with 5% CO_2. The cells were obtained courtesy of Dr. Martin Pomper, Johns Hopkins University.[15] According to experimental protocols of the respective cell assay mentioned in the Supporting Information, cells were trypsinized (0.25%) for 2–3 min to detach from the culture flasks for further passage or to seed the cells in suitable multiwell plates to perform cell binding assays.

Competition Radioligand Binding Assay: The protocol for the production of [^{68}Ga]PSMA-11 and competition radioligand binding assay to calculate the IC_{50} values were followed as per prior reports.[12,16] [^{68}Ga]PSMA-11, produced at the Department of Radiology, UCSF for clinical use, was procured and used in the competition radioligand binding assay to acquire the IC_{50} values for the nanocarriers.[16] Briefly, around ≈0.185 megabecquerel (MBq) (2.5 ng) of [^{68}Ga]PSMA-11 along with different concentrations (0.01×10^{-9}–$100\,000 \times 10^{-9}$ M) of the nonradiolabeled nanocarriers was added to each well of a 96-well plate seeded with PSMA+ PC3-Pip cells (~20k cells per wells). After 1 h incubation at room temperature, the radioactive medium was removed, and the cells were washed with phosphate-buffered saline (PBS) twice. The cells were lysed with sodium hydroxide and the radioactivity of the lysate in each well was quantified in a Hidex gamma counter. IC_{50} was determined by nonlinear regression analysis in Prism software (Graph-Pad).

^{177}Lu Radiolabeling of StarPEGs: StarPEG nanocarrier in water was added to a solution of 10×10^{-3} M NH_4OAc containing 10 vol% of ascorbic acid (20 mg mL^{-1}) and $^{177}LuCl_4$ in a ratio of 0.37 MBq μg^{-1} of nanocarriers were mixed to it. The mixture was incubated for 1 h at 55 °C (Thermal mixture, Fisher Scientific, Hampton, NH). The radiolabeled product was purified using PD-10 size-exclusion desalting column (Fisher Scientific), by equilibrating and eluting with saline solution containing 0.2 mg of L-ascorbic acid per milliliter. Instant thin layer chromatography (iTLC) was performed using silica gel-impregnated glass microfiber chromatography paper (Neta Scientific, Hainesport, NJ) and developed with 20×10^{-3} M citric acid solution to confirm radiolabeling purity. Multiple radiolabeling studies were carried out with different amounts of nanocarriers and ^{177}Lu, as summarized in Table S1 (Supporting Information).

^{177}Lu Radiolabeling of PSMA-617: The radiolabeling of PSMA-617 with ^{177}Lu and its purification was performed following previously reported protocols.[17] PSMA-617 in water (25 µg per 25 µL) was added to 925 MBq of ^{177}Lu in 250 µL 0.18 M ascorbic acid solution and the solution was shaken at 95 °C for 40 min (Thermal mixture, Fisher Scientific). iTLC was carried out using glass microfiber chromatography paper impregnated with silica gel with 5×10^{-3} M ethylenediaminetetraacetic acid (EDTA) (pH 5.5) to confirm radiolabeling purity. Purification was performed with a C-18 light cartridge (Fisher Scientific) equilibrated with 5 mL of 70% EtOH followed by 10 mL of H_2O. The reaction mixture was diluted with saline to 1 mL, loaded to the cartridge and washed with 5 mL saline to remove impurities and free ^{177}Lu. Followed by the washing, the cartridge was eluted with 1 mL of 70% EtOH to collect pure [^{177}Lu]PSMA-617. [^{177}Lu]PSMA-617 was blow-dried under vacuum to remove EtOH and the desired aliquot was prepared in saline solution containing 0.2 mg mL^{-1} ascorbic acid. The isolated radiochemical yield after cartridge purification was 90%, with greater than 95% purity and molar activity was 41.68 MBq $nmol^{-1}$.

In Vitro Cell Binding Assay: The in vitro saturation binding assay, blocking assay, and membrane-bound and internalization assay were performed as per our prior report.[12] The detail protocol included in the Supporting Information. Saturation binding assay was conducted to estimate the equilibrium dissociation constant (K_d) to evaluate and rank order strengths of target binding affinity. By using a standard target binding agent as blocking agent, the blocking assay was performed to confirm the specificity of the investigational radiopharmaceutical for PSMA. In contrast, the membrane-bound and internalization assay helps in quantifying the fraction of the radiopharmaceutical which remains bound to the surface or internalized.

In Vitro Colony Formation Assay: Both PSMA+ PC3-Pip and PSMA– PC3-Flu cells were seeded in 6-well tissue culture plate at 200 cells per well in triplicates. The cells were treated with different doses (0–10 MBq mL^{-1}) of the PSMA targeted nanocarrier [^{177}Lu]PEG-$(DOTA)_1(ACUPA)_3$. After 96 h of drug treatment, the cells were washed with PBS twice and fresh media was added and cells were incubated to let the colony grow. Post 12 days of incubation, the media was removed and colonies were fixed with 4% formaldehyde. The colonies were stained with 1% w/v crystal violet (in 4% paraformaldehyde) for 15 min. Following this, colonies were washed with PBS, and number of colonies were counted using Image J.

Inoculation of Mice with Dual Xenograft and Metastatic Tumors: The in vivo animal studies were performed under a protocol (AN191219-01ZL) approved by the UCSF Institutional Animal Care & Use Committee (IACUC). Using the same protocol from our prior report, homozygous (nu/nu) athymic male mice of 4–5 weeks old (Jackson Laboratories or Envigo-Harlan Laboratories, Livermore CA) were inoculated with PC3-Pip (left flank, 1 million cells) and PC3-Flu (right flank, 1 million cells) dual xenografts were generated.[12] The tumor size was approximately 100–200 mm^3 1–2 weeks post-inoculation.

Metastatic models were obtained by injecting 1 million PC3-Pip cells by intracardiac injection (in 100 µL PBS) into the left ventricle of the heart of homozygous (nu/nu; strain#: 0 02019) athymic male mice of 6–8 weeks old. Intracardiac injections were performed by the UCSF Preclinical Therapeutic Core. In brief, mice were subjected to an echocardiographic exam followed by an intraventricular injection of tumor cells. After anesthesia induction with isoflurane (Isoflo, Zoetis. Parsippany, New Jersey, USA) at 4% in fresh oxygen, animals were placed in dorsal recumbency on the exploratory platform and isoflurane reduced to 2% for maintenance. The ultrasonographic gel was applied over the chest and an examination was performed looking for the left ventricle on the left side of the thorax, over the sternum. Once the targeted structure was located, the scanning probe was fixed and the injection needle was firmly introduced into the left ventricle through an intercostal space. The injection was confirmed when the needle tip was seen inside the left ventricle under the papillary muscles. After that, cells were slowly injected and visible as small hyperechoic dots arising inside the anechoic ventricular chamber. Once the injection was finished, the needle was gradually removed from the heart and the mouse was placed in a warm cage for recovery. The tumor growth was monitored by [^{68}Ga]PSMA-11 µPET/CT at multiple time points after the intraventricular injection of tumor cells.

In Vivo µSPECT/CT Imaging and Biodistribution Studies: One week post-inoculation, when tumors were approximately 100–200 mm^3, the animals were anesthetized using 2% isoflurane and the respective ^{177}Lu radiolabeled StarPEG nanocarriers were administered via tail vein. An amount of 38.48–43.29 MBq in 100 µL of saline per mouse was injected for µSPECT (micro single-photon emission computed tomography)/CT imaging (two groups of four mice), whereas around 9–10 MBq in 100 µL of saline per mouse was injected for ex vivo biodistribution (two groups of six mice each). The mice were scanned at 24, 72, 144, and 192 h post radiopharmaceutical injection in a µSPECT/CT imaging system (VECTor4CT, MIL-

abs, BV). Image reconstruction was performed using a vendor-provided ordered subsets expectation maximization (OSEM) algorithm. CT-based attenuation correction and energy-window-based scatter correction were performed and the raw reconstructed pixel value to a physical unit of Bq mL^{-1} was performed using a precalibrated conversion factor. The imaging data was processed and viewed in an open-source AMIDE software (http://amide.sourceforge.net/). The tumor-bearing mice injected with 9–10 MBq of ^{177}Lu radiolabeled StarPEG nanocarriers were sacrificed at 72 h ($n = 3$) and 192 h ($n = 3$). Blood was collected through a cardiac puncture and major organs (liver, kidney, spleen, heart, pancreas, lung, brain, femur, muscle, testis, and subcutaneous tumor) were harvested. Blood and major organs were weighed and analyzed in an automated gamma counter (Hidex, Turku, Finland). The percent injected dose per gram of tissue (% ID g^{-1}) was determined by comparing standard radioactivity.

Tumor and Normal Tissue Radiation Dose Estimation: Spherical VOIs were drawn on coregistered CT images for tumors at all time points. All VOIs were spheres (2 mm diameter) and placed well within the anatomical boundaries to minimize spill-over or spill-in of radioactivity. The percent of injected activity (%IA) for a normalized volume (0.5 mL) at each time point was computed for curve-fitting to derive TIACs and the dose (mGy MBq^{-1}) was calculated for a sphere model. The estimation of normal tissue radiation dose was performed as per the prior report.[18,19]

Autoradiography: After analyzing the dissected organ samples in the gamma counter (Hidex), the tumors were embedded in optimal cutting temperature (OCT) compound and flash frozen on dry ice. Using a microtome, the frozen tumor tissues were sectioned at 20 µm thickness and mounted on iQID charged-particle digital autoradiography imaging systems (QScint Imaging Solutions, LLC, Tucson, AZ). The raw autoradiography data were processed in ImageJ software.

Treatment Studies: For the treatment studies, each mouse's body weight and tumor measurements were performed until the mice reached a humane endpoint including body condition score below 2, weight loss by 20%, or tumor volume of 2000 mm^3. The tumor measurements were carried out twice a week and tumor volumes were calculated by the formula $V = [\text{length} \times (\text{width})^2]/2$.

Animals were randomized in groups of $n = 10$ and injections were performed when the tumor reached 100 mm^3. The PC3-Pip xenograft-bearing mice were injected with a single dose of vehicle, 4.6, 9.2, or 18.5 MBq of [^{177}Lu]PEG-$(DOTA)_1(ACUPA)_3$. In addition, a separate group received a 9.2 MBq dose of [^{177}Lu]PSMA-617. In the [^{177}Lu]PSMA-617 and 18.5 MBq [^{177}Lu]PEG-$(DOTA)_1(ACUPA)_3$ arms, one cage of $n = 5$ each developed severe *Corynebacterium Bovis* infection and had to be euthanized. These were excluded from further analysis.

For PC3-Pip metastatic models, the mice were either treated with a single dose of vehicle or 9.2 MBq of [^{177}Lu]PEG-$(DOTA)_1(ACUPA)_3$. The body weights for each mouse were measured until the mice reached a humane endpoint including body condition score below 2, weight loss by 20%. Mice were imaged with [^{68}Ga]PSMA-11 PET/CT at days −1, 18, and 35. Surviving mice underwent biodistribution study following [^{68}Ga]PSMA-11 administration on days 35 and 50.

Chronic Toxicity Study: The nude mice bearing PC3-Pip subcutaneous tumors which were treated with different doses of [^{177}Lu]PEG-$(DOTA)_1(ACUPA)_3$ survived until 138 days post-treatment and were euthanized at that time point to analyze toxicity of the treatment. A complete blood count and laboratory liver and kidney function tests were conducted to study chronic toxicity. Blood was collected by cardiac puncture in EDTA-coated tubes to study blood cell counts. Small fractions of blood were allowed to sit at 4 °C for 30 min in vials and the clotted blood samples were centrifuged (10 000 x *g*, 10 min, at 4 °C) to separate the serum. Blood and serum samples were sent to the Comparative Pathology Laboratory, UC Davis School of Veterinary Medicine for blood cell counts and organ function tests.

Histology of the Tissue Sections: Following organ biodistribution, the tissue sections of thickness 10 µm were collected from OCT-embedded frozen organ samples on glass slides. Routine histologic analysis was performed to study microscopic features of the tumor samples. The tissue sections were shocked in acetone at −20 °C for 20 min followed by in methanol at 4 °C for 10 min. The tissue sections were then rehydrated with water and treated with hematoxylin (5 min), bluing reagent (10 s) and eosin (30 s) followed by washing with water after each treatment. The stained tissue was washed with ethanol (50%, 70%, and 95%) for 2 min each, followed by xylene treatment for 5 min and the mounting medium was applied.

Statistical Analysis: All data are presented as mean ± standard deviation in plots. The data were subjected to Student's *t*-test (unpaired, two-tailed, equal variance) for statistical analysis. To compare the blood cells and liver and kidney function tests between saline control and treated groups, one-way ANOVA was used with Dunnett multiple comparisons test. Differences at the 95% confidence level ($p < 0.05$) are considered to be statistically significant.

Ethics Approval and Consent to Participate: All animal experiments were carried out in accordance with University of California, San Francisco Institutional Animal Care & Use Committee (IACUC) under protocol number AN191219-01ZL.

Supporting Information

Supporting Information is available from the Wiley Online Library or from the author.

Acknowledgements

The authors thank Dr. Martin Pomper, Johns Hopkins University, for the PC3-Pip and PC3-Flu cell lines and the U. S. Department of Energy Isotope Program is acknowledged for 177Lu production. This project was funded by the Cancer Center Support Grant P30CA082103, U. S. Department of Defense Translational Science Award W81XWH-20-1-0292 (RRF), R01CA266666 (HFV, RRF, RA), S10OD012301 (YS), and the Cancer League (RRF) and the Precision Imaging of Cancer Therapy program (HV). N.M. thanks the Department of Science and Technology (DST), India, for the INSPIRE Faculty Fellowship.

Conflict of Interest

A patent has been filed describing the nano polymers detailed in the publication.

Author Contributions

Conceptualization, investigation, methodology, laboratory research, data curation, software, formal analysis, validation, project administration, writing-original draft, and reviewing and editing manuscript were performed by N.M. Methodology, laboratory research, data curation, formal analysis, validation, and reviewing and editing manuscript were performed by G.W.A., K.N.B., A.W., A.P.B., and C.D. Methodology, data curation, and formal analysis were performed by C.M., J.A.C.S., A.R., and D.P.B. Formal analysis was performed by R.A.S. and N.Y.G. Reviewing and editing manuscript was performed by A.O., D.M.W., Y.S., and D.V.S. Conceptualization, resources, investigation, methodology, formal analysis, validation, visualization, project administration, reviewing and editing manuscript, supervision, and funding acquisition were performed by H.F.V. Conceptualization, resources, investigation, methodology, formal analysis, validation, visualization, project administration, writing-original draft, reviewing and editing manuscript, supervision, and funding acquisition were performed by R.R.F.

Data Availability Statement

The data that support the findings of this study are available from the corresponding author upon reasonable request.

Keywords

enhanced permeability and retention, polymer nanocarriers, prostate cancer, prostate-specific membrane antigen (PSMA), radioligand therapy, single photon excited computed tomography (SPECT) imaging

Received: December 25, 2023
Revised: April 29, 2024
Published online:

[1] H. Wang, Z. He, X. Liu, Y. Huang, J. Hou, W. Zhang, D. Ding, *Small Struct.* **2022**, *3*, 2200036.
[2] M. Davis, M. Bennett, L. Thomas, P. Bjorkman, *Proc. Natl. Acad. Sci. USA* **2005**, *102*, 5981.
[3] *J. Nucl. Med.* **2022**, *63*, 13N.
[4] a) S. Pastorino, M. Riondato, L. Uccelli, G. Giovacchini, E. Giovannini, V. Duce, A. Ciarmiello, *Curr. Radiopharm.* **2020**, *13*, 63; b) L. Filippi, A. Chiaravalloti, O. Schillaci, O. Bagni, *Expert Rev. Anticancer Ther.* **2020**, *20*, 823.
[5] a) E. Price, C. Orvig, *Chem. Soc. Rev.* **2014**, *43*, 260; b) M. Hofmann, H. Maecke, A. Borner, E. Weckesser, P. Schoffski, M. Oei, J. Schumacher, M. Henze, A. Heppeler, G. Meyer, W. Knapp, *Eur. J. Nucl. Med.* **2001**, *28*, 1751; c) D. Debela, S. Muzazu, K. Heraro, M. Ndalama, B. Mesele, D. Haile, S. Kitui, T. Manyazewal, *SAGE Open Med.* **2021**, *9*, 20503121211034366.
[6] N. Meher, H. F. VanBrocklin, D. M. Wilson, R. R. Flavell, *Pharmaceuticals.* **2023**, *16*, 315.
[7] H. Maeda, J. Wu, T. Sawa, Y. Matsumura, K. Hori, *J. Controlled Release.* **2000**, *65*, 271.
[8] H. Maeda, *Adv. Drug Delivery Rev.* **2015**, *91*, 3.
[9] J. Goos, A. Cho, L. Carter, T. Dilling, M. Davydova, K. Mandleywala, S. Puttick, A. Gupta, W. Price, J. Quinn, M. Whittaker, J. Lewis, T. Davis, *Theranostics.* **2020**, *10*, 567.
[10] A. E. Hansen, A. L. Petersen, J. R. Henriksen, B. Boerresen, P. Rasmussen, D. R. Elema, P. M. af Rosenschöld, A. T. Kristensen, A. Kjær, T. L. Andresen, *ACS Nano.* **2015**, *9*, 6985.
[11] D. Vera, S. Fontaine, H. VanBrocklin, B. Hearn, R. Reid, G. Ashley, D. Santi, *Mol. Cancer Ther.* **2020**, *19*, 673.
[12] N. Meher, G. Ashley, A. Bidkar, S. Dhrona, C. Fong, S. Fontaine, D. Vera, D. Wilson, Y. Seo, D. Santi, H. VanBrocklin, R. Flavell, *ACS Appl. Mater. Interfaces.* **2022**, *14*, 50569.
[13] J. Lim, B. Guan, K. Nham, G. Hao, X. Sun, E. Simanek, *Biomolecules.* **2019**, *9*, 421.
[14] C. Heneweer, J. Holland, V. Divilov, S. Carlin, J. Lewis, *J. Nucl. Med.* **2011**, *52*, 625.
[15] a) Z. Chen, M. Penet, S. Nimmagadda, C. Li, S. Banerjee, P. Winnard, D. Artemov, K. Glunde, M. Pomper, Z. Bhujwalla, *ACS Nano.* **2012**, *6*, 7752; b) W. Lesniak, S. Boinapally, S. Banerjee, B. Azad, C. Foss, C. Shen, A. Lisok, B. Wharram, S. Nimmagadda, M. Pomper, *Mol. Pharmaceutics.* **2019**, *16*, 2590.
[16] a) N. Meher, K. Seo, S. Wang, A. Bidkar, M. Fogarty, S. Dhrona, X. Huang, R. Tang, C. Blaha, M. Evans, D. Raleigh, Y. Jun, H. VanBrocklin, T. Desai, D. Wilson, T. Ozawa, R. Flavell, *ACS Appl. Mater. Interfaces.* **2021**, *13*, 54739; b) R. Nanabala, M. Anees, A. Sasikumar, A. Joy, M. Pillai, *Nucl. Med. Biol.* **2016**, *43*, 463.
[17] K. Eryilmaz, B. Kilbas, *EJNMMI Radiopharm. Chem.* **2021**, *6*, 16.
[18] M. Evans, Y. Huang, C. Drake, *20220280661*, **2022**.
[19] J. Violet, P. Jackson, J. Ferdinandus, S. Sandhu, T. Akhurst, A. Iravani, G. Kong, A. R. Kumar, S. P. Thang, P. Eu, M. Scalzo, D. Murphy, S. Williams, R. J. Hicks, M. S. Hofman, *J. Nucl. Med.* **2019**, *60*, 517.
[20] J. Jewett, C. Bertozzi, *Chem. Soc. Rev.* **2010**, *39*, 1272.
[21] C. Choy, X. Ling, J. Geruntho, S. Beyer, J. Latoche, B. Langton-Webster, C. Anderson, C. Berkman, *Theranostics.* **2017**, *7*, 1928.
[22] a) S. Maus, E. d. Blois, S. J. Ament, M. Schreckenberger, W. A. P. Breeman, *Int. J.* **2014**, *1*, 5; b) E. A. M. Ruigrok, N. van Vliet, S. U. Dalm, E. de Blois, D. C. van Gent, J. Haeck, C. de Ridder, D. Stuurman, M. W. Konijnenberg, W. M. van Weerden, M. de Jong, J. Nonnekens, *Eur. J. Nucl. Med. Mol. Imaging.* **2021**, *48*, 1339.
[23] a) S. Wang, C. Blaha, R. Santos, T. Huynh, T. Hayes, D. Beckford-Vera, J. Blecha, A. Hong, M. Fogarty, T. Hope, D. Raleigh, D. Wilson, M. Evans, H. VanBrocklin, T. Ozawa, R. Flavell, *Mol. Pharmaceutics.* **2019**, *16*, 3831; b) S. Wang, J. Li, J. Hua, Y. Su, D. Beckford-Vera, W. Zhao, M. Jayaraman, T. Huynh, N. Zhao, Y. Wang, Y. Huang, F. Qin, S. Shen, D. Gioeli, R. Dreicer, R. Sriram, E. Egusa, J. Chou, F. Feng, J. He, *Clin. Cancer Res.* **2021**, *27*, 1305.
[24] J. Mesters, K. Henning, R. Hilgenfeld, *Acta Crystallogr., Sect. D: Struct. Biol.* **2007**, *63*, 508.
[25] K. Maresca, S. Hillier, F. Femia, D. Keith, C. Barone, J. Joyal, C. Zimmerman, A. Kozikowski, J. Barrett, W. Eckelman, J. Babich, *J. Med. Chem.* **2009**, *52*, 347.
[26] S. Boinapally, A. Lisok, G. Lofland, I. Minn, Y. Yan, Z. Jiang, M. J. Shin, V. F. Merino, L. Zheng, C. Brayton, M. G. Pomper, S. R. Banerjee, *Eur. J. Nucl. Med. Mol. Imaging.* **2022**, *49*, 4369.
[27] K. Sjögreen Gleisner, N. Chouin, P. M. Gabina, F. Cicone, S. Gnesin, C. Stokke, M. Konijnenberg, M. Cremonesi, F. A. Verburg, P. Bernhardt, U. Eberlein, J. Gear, *Eur. J. Nucl. Med. Mol. Imaging.* **2022**, *49*, 1778.
[28] V. J. Tschan, F. Borgna, S. D. Busslinger, M. Stirn, J. M. M. Rodriguez, P. Bernhardt, R. Schibli, C. Müller, *Eur. J. Nucl. Med. Mol. Imaging.* **2022**, *49*, 3639.
[29] C. A. Manuel, U. Pugazhenthi, S. P. Spiegel, J. K. Leszczynski, *J. Am. Assoc. Lab. Anim. Sci.* **2017**, *56*, 202.
[30] J. M. Kelly, A. Amor-Coarasa, S. Ponnala, A. Nikolopoulou, C. Williams, S. G. DiMagno, J. W. Babich, *J. Nucl. Med.* **2019**, *60*, 656.
[31] A. P. Bidkar, S. Wang, K. N. Bobba, E. Chan, S. Bidlingmaier, E. A. Egusa, R. Peter, U. Ali, N. Meher, A. Wadhwa, S. Dhrona, C. Dasari, D. Beckford-Vera, Y. Su, R. Tang, L. Zhang, J. He, D. M. Wilson, R. Aggarwal, R. R. Flavell, *Clin. Cancer Res.* **2023**, *29*, 1916.